SNAT-YOLO: Efficient Cross-Layer Aggregation Network for Edge-Oriented Gangue Detection

Shang Li
Anhui University of Science & Technology
19803299203@163.com

Abstract

To address the issues of slow detection speed, low accuracy,challenging to deploy on industrial edge devices,and large parameter and computational requirements in deep learning-based coal gangue target detection methods, we propose a lightweight coal gangue target detection algorithm based on an improved YOLOv11. First, we use the lightweight network ShuffleNetV2 as the backbone to enhance the detection speed. Second, we introduce a lightweight down sampling operation, ADown, which reduces model complexity while improving the average detection accuracy. Third, we improve the C2PSA module in YOLOv11 by incorporating the Triplet Attention mechanism, resulting we propose a model named C2PSA-TriAtt module, which enhances the model's ability to focus on different dimensions of the images. Fourth, we propose the Inner-FocalerIoU loss function to replace the existing CIoU loss function. Experimental results show that our model achieves a detection accuracy of 99.10% in coal gangue detection tasks, reduces the model size by 38%, the number of parameters by 41%, and the computational cost by 40%, while decreasing the average detection time per image by 1 ms. The improved model demonstrates enhanced detection speed and accuracy, making it suitable for deployment on industrial edge mobile devices, thus contributing positively to coal processing and the efficient utilization of coal resources.

1. Introduction

1.1. Research Background

China's energy structure dictates that coal will remain the primary source of energy consumption for the foreseeable future [1]. During the coal mining process, coal gangue, a by-product, is commonly mixed with coal and its large-scale accumulation has become one of the main solid pollutants threatening the ecological environment [2]. With the increasing awareness of environmental protection and the growing demand for resource recovery, the efficient sorting and processing of coal gangue have not only become an important industry issue but also play a crucial role in promoting the clean utilization of coal [3]. Current technological developments show a clear trend: deep learning-based artificial intelligence recognition methods are gradually becoming mainstream. Compared to traditional physical detection methods such as density and hardness identification, and gangue identification methods based on grayscale and texture features, deep learning methods exhibit significant advantages in feature extraction and pattern recognition [4].

In recent years, the continuous optimization and upgrading of the mining and processing systems have increasingly focused on clean and efficient handling while ensuring economic development. As a solid waste product associated with coal mining and processing, coal gangue has a low calorific value and accounts for about 15% of the total raw coal production [5]. Gangue mixed with coal not only significantly reduces combustion efficiency [6] but also releases large amounts of harmful gases during combustion, causing severe environmental pollution [7]. Given the ongoing support of the coal industry to the national economy, achieving efficient gangue separation has become a key technical challenge that balances economic benefits and environmental governance.

The current gangue separation technology system mainly includes three categories:

Manual Sorting Method: This method relies on workers' experience to sort large pieces of gangue [8]. It has inherent drawbacks such as poor working conditions and low sorting accuracy.

Wet Separation Technology: This method separates coal and gangue through the density difference in water media [15]. However, since 70% of China's coal resources are located in arid and water-scarce western regions [14], this method faces practical constraints such as elevated water consumption and wastewater treatment costs.

Dry Separation Technology: Dry coal beneficiation is also a commonly employed coal preparation method in China

[13].This category includes wind sorting based on gas-solid two-phase flow dynamics [10], ray identification utilizing differences in atomic numbers [9],machine vision sorting based on optical sensing [11], and sorting using infrared image recognition technology [12]. The advancement in computer hardware, marked by the performance leap in GPUs/CPU [16], has driven breakthroughs in deep learning and convolutional neural networks in the field of image recognition. This provides a solid technical foundation for building intelligent recognition systems for coal gangue based on deep learning. Compared to traditional physical separation methods, these systems exhibit significant advantages in feature extraction and pattern recognition accuracy,making them valuable for engineering applications.

1.2. Related Work

In recent years, with the rapid development of artificial intelligence technology, deep learning-based image recognition techniques have provided strong support for the rapid identification of coal gangue. Many researchers have applied deep learning techniques to coal gangue recognition, including convolutional neural networks (CNN), transfer learning, and data augmentation. For example, Jia et al. [17] proposed a lightweight coal gangue recognition method named S3DD-YOLOv8, which improves the performance of the network model while maintaining moderate increases in model parameters and complexity, leading to higher accuracy compared to the original model. Lei et al. [18] improved YOLOv3-M, accelerating the convergence speed on small samples and enhancing recognition accuracy. Sui et al. [19] modified the spatial pyramid pooling structure of the YOLOv7-tiny algorithm, improving overall detection accuracy. Zhang et al. [20] enhanced the YOLOv5 model using the AdaBelief optimization algorithm, resulting in a 2.27% improvement in recognition accuracy. Chang et al. [21] proposed a coal gangue recognition method using an improved YOLOv5m model with DIOU-NMS recognition accuracy enhancement, leading to improved tracking frame accuracy. Shen et al. [22] proposed an improved YOLOv5s algorithm that enhances mean accuracy by 1.7% through linear scaling of anchor boxes obtained by the K-means clustering algorithm. Zeng et al. [23] used the Our-v8 model, introducing the CBAM attention mechanism and an improved EIOU loss function in the YOLOv8 model, achieving an average detection accuracy of 99.50%. Yan et al. [32] proposed the Yolov8n-FEL model, combining multi-spectral imaging technology to increase the model's average precision to 98.90% and reduce the model size to 5.07 MB.

Despite the improvements in coal gangue recognition accuracy achieved by previous studies, some limitations remain. For instance, increased model parameters and longer running times, as well as lower detection accuracy for miniature targets in the YOLOv5 model. The CIOU_Loss method, which optimizes detection by calculating the overlap area between the detection box and the ground truth box, performs poorly when the detection box and the ground truth box are nested [26]. Additionally, the loss function converges slowly in horizontal and vertical directions, which is detrimental to the classification of coal gangue. Furthermore, although the research results have made progress on the original basis, there is still considerable room for improvement. For example, the Our-v8 model proposed by Zeng et al. [23] achieves an average detection accuracy of 99.50%, but the model parameter size is as high as 12.8M, and the model volume is 22.1MB.

Therefore, we propose a model named SNAT-Yolo. We have made lightweight improvements to the YOLOv11 model by replacing its backbone network with ShuffleNetv2 to reduce the number of model parameters and using a lightweight down sampling operation ADown to enhance detection accuracy while reducing model parameters. Additionally, we use a triple self-attention mechanism to improve the C2PSA module, enabling the network to comprehensively understand image content. Finally, we introduce the Inner-Focaler loss function to replace the original CIou loss function, addressing issues of sample imbalance and achieving faster convergence and more accurate regression results.

2. Method

2.1. YOLOv11 Model

In this study, the YOLOv11 model is utilized for coal gangue target detection. As the latest version of the YOLO series [24], YOLOv11 retains its fast end-to-end detection characteristics while introducing several improvements to balance speed and accuracy [25]. YOLOv11 introduces the C3k2 mechanism to replace the original C3k mechanism and incorporates the C2PSA multi-head attention mechanism. Additionally, a DWConv (Depthwise Convolution) is added to the classification detection head in the decoupled head to enhance computational efficiency and reduce the number of paramet

ers. Furthermore, the "single-stage" design allows the prediction of multiple targets and categories through a single forward pass of the network, making it highly efficient and particularly suitable for complex coal gangue detection tasks. The specific network architecture of YOLOv11 is shown in Figure 1.

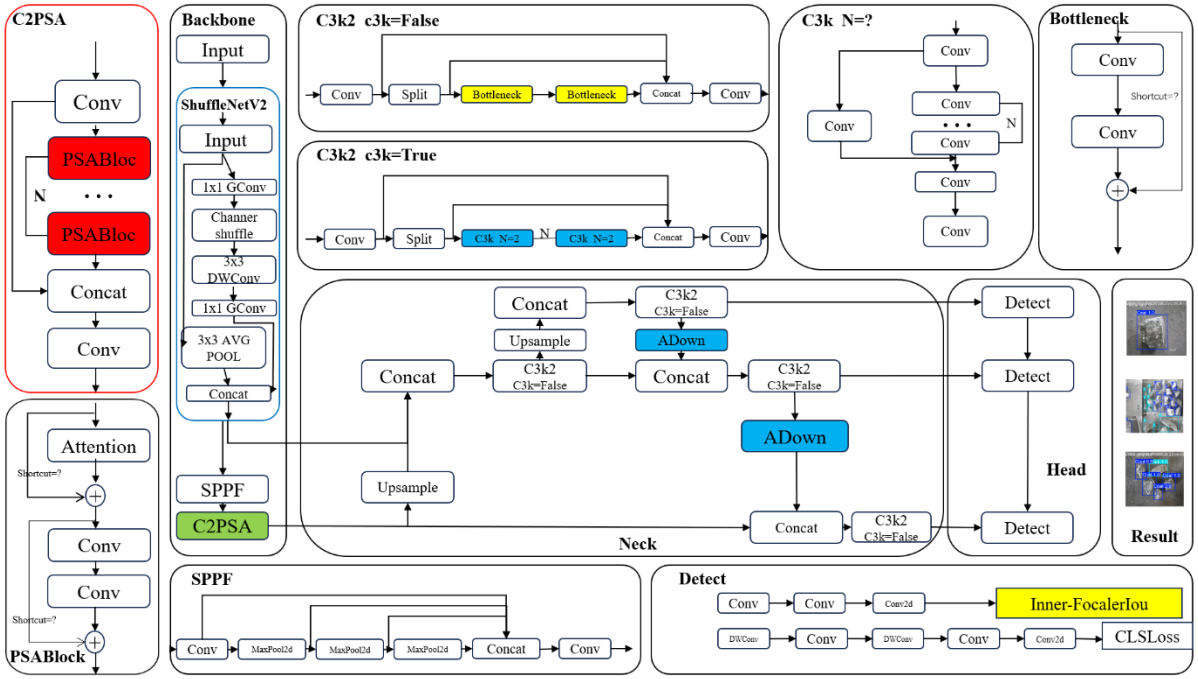

Figure 1. YOLOv11 Network Architecture

2.2. Improved YOLOv11 Model

We have made the following improvements to YOLOv11. The ShuffleNetV2 network, proposed by Ma et al. [27], is an efficient CNN architecture designed for mobile devices. It emphasizes not only FLOPs but also speed, memory access cost, and platform characteristics, building upon the foundation of ShuffleNetV1. By using new operations such as pointwise group convolution and channel shuffle, it reduces computational costs while maintaining network accuracy. Comprehensive experiments have shown that ShuffleNetV2 significantly outperforms existing efficient models in coal gangue detection tasks, providing better speed-capacity trade-offs.

The ADown module, introduced by Wang et al. [28], is a convolutional block used for down sampling operations in object detection tasks. In deep learning models, down sampling is a common technique to reduce the spatial dimensions of feature maps, which helps the model capture higher-level features of images while reducing computational load. The ADown module is designed to perform this operation efficiently with minimal impact on performance. It primarily consists of three parts: convolution operations, stride adjustments, and numerical optimization, all aimed at enhancing model performance.

Triplet Attention, proposed by Misra et al. [30], is a self-attention mechanism that provides the ability to build dependencies between channels or spatial positions. Triplet Attention captures interactions across the channel, height, and width dimensions through an innovative three-branch structure. It computes attention weights by rotating the input tensor and applying residual transformations to establish dependencies across different dimensions. This enhances the network's ability to capture cross-dimensional dependencies when computing attention weights.

To address the issue of insufficient accuracy in bounding box regression (BBR) in object detection, Zhang et al. [29] proposed InnerIoU. Traditional IoU (Intersection over Union) computation considers the overall overlap region between predicted and ground truth bounding boxes, whereas InnerIoU focuses on the overlapping area inside the bounding boxes. It achieves this by introducing auxiliary bounding boxes, which are smaller versions of the original bounding boxes, for the purpose of loss function calculation.

Focaler-IoU, a loss function for bounding box regression in object detection, was introduced by Zhang et al. [30]. Focaler-IoU improves detector performance in various detection tasks by focusing on different regression samples. This is ac

hieved through linear interval mapping to reconstruct the IoU loss, thereby paying attention to different samples. It analyzes and considers the distribution of difficult and easy samples in bounding box regression, an aspect often overlooked in existing IoU loss functions. Focaler-IoU addresses the shortcomings of existing bounding box regression methods, thus further enhancing detection performance in various tasks.

Therefore, we first replaced the entire backbone network of YOLOv11 with the ShuffleNetV2 network. Second, we improved the C2PSA module using Triplet Attention, proposing the C2PSA-TriAtt module. Third, we enhanced the neck structure of YOLOv11 by incorporating the ADown down sampling operation. Finally, we combined InnerIoU and Focaler-IoU to propose the Inner-FocalerIoU loss function, replacing the original CIoU loss function. In summary, we proposea new coal gangue detection algorithm named SNAT-YOLO.The improved YOLOv11 network architecture is illustrated in Figure 2.

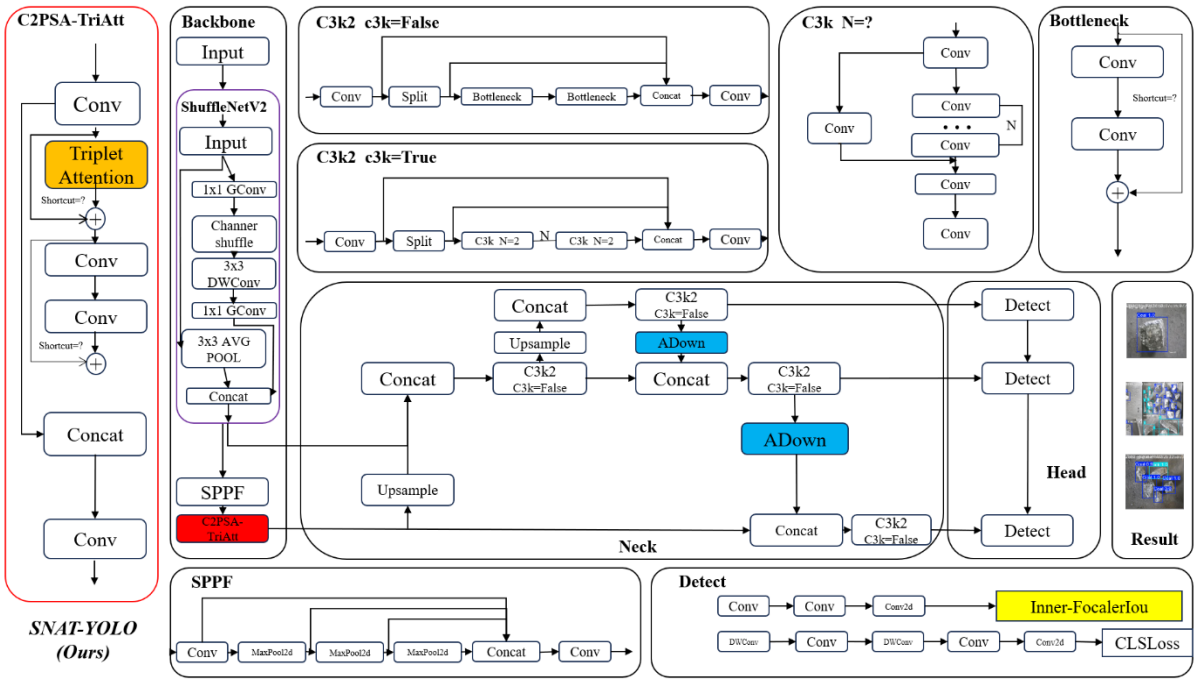

Figure 2. SNAT-YOLO: Improved YOLOv11 Network Architecture

2.3. ShuffleNetV2

ShuffleNetV2 is designed to reduce computational costs while maintaining network accuracy by utilizing pointwise group convolution and channel shuffle operations [27]. The mechanism of channel shuffle in ShuffleNetV2 is illustrated in Figure 3.

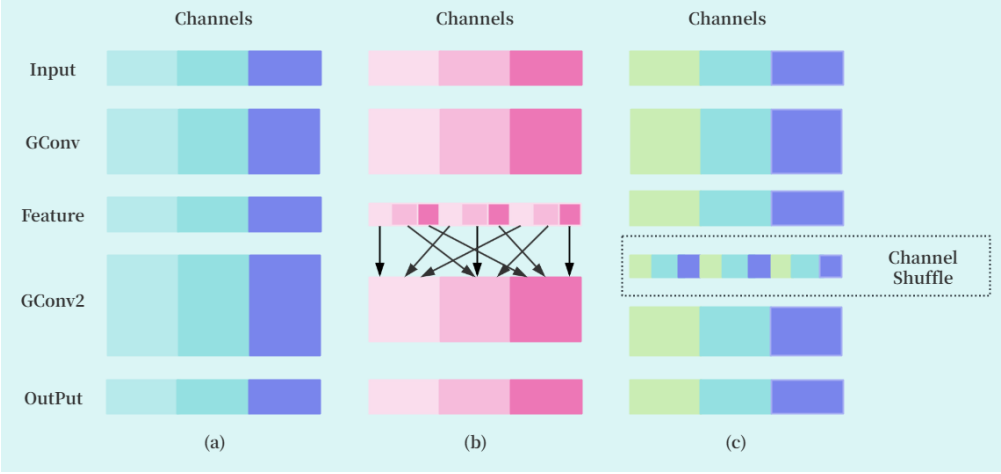

Figure 3. Channel Shuffle Mechanism

In Figure 3. , the channel shuffle operation is achieved through two stacked group convolutions (GConv), which serve the following purposes:(a): Two stacked convolution layers with the same number of groups are shown. Each output channel is only associated with input channels within the same group.(b): Without channel shuffle, it demonstrates how input and output channels are fully correlated when GConv2 fetches data from different groups after GConv1.(c): This is the same implementation as (b), but with channel shuffle applied to allow cross-group communication, enabling more effective and robust feature learning within the network.

The ShuffleNetV2 unit is derived from the basic bottleneck unit, and the specific structure of the ShuffleNetV2 unit in ShuffleNetV2 is shown in Figure 4.

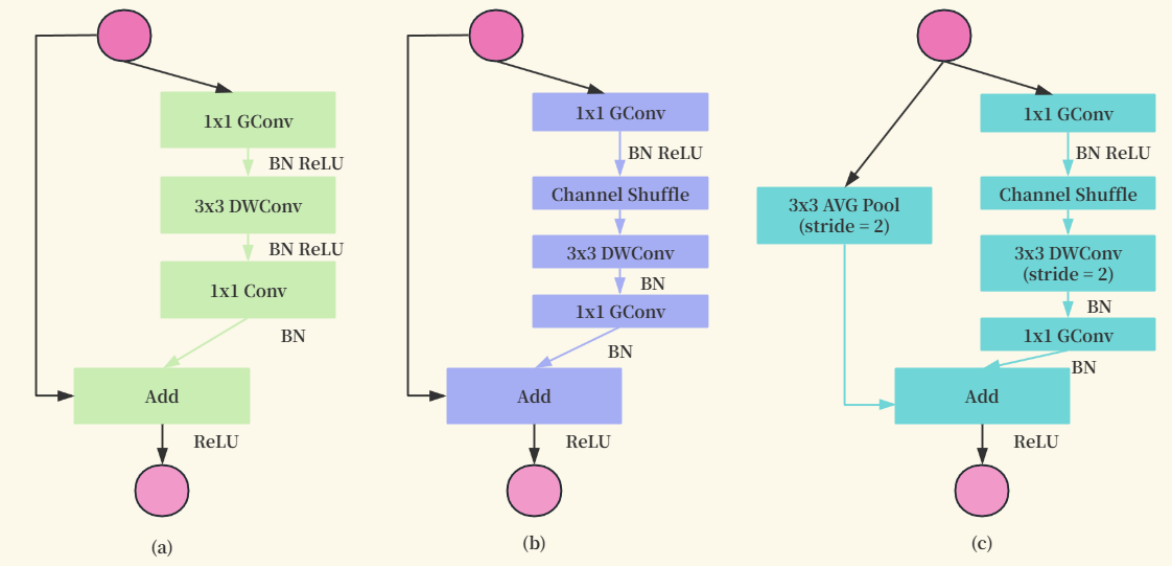

Figure 4. ShuffleNetV2 Unit Structure

(a): A basic bottleneck unit is shown, which uses depthwise separable convolution (DWConv) and a simple addition (Add) to fuse features.(b): Based on the standard bottleneck unit, pointwise group convolution (GConv) and channel shuffle operations are introduced to enhance feature representation.(c): This is the ShuffleNetV2 unit designed for spatial down sampling. To reduce memory access costs, ShuffleNetV2 does not include excessive convolution groups. Instead, it uses a stride-2 average pooling (AVG Pool) and depthwise separable convolution, followed by channel shuffle and pointwisegroup convolution to further process features. Finally, features are merged through a concatenation operation (Concat).The memory access cost of the convolution group is expressed by Eq. 1, where c_1 represents the number of input channels, c_2 represents the number of output channels, and hw represents the size of the spatial map.

$$MAC = hw(c_1 + c_2) + \frac{c1c2}{g} \quad (1)$$

After replacing the backbone of YOLOv11 with ShuffleNetV2, we found that the model's computational cost and parameters were reduced, while the detection accuracy and performance remained largely unchanged.

2.4. C2PSA-TriAtt

The basic principle of the Triplet Attention mechanism is to capture cross-dimensional interactions of input data using a three-branch structure, thereby computing attention weights [30]. This method can build dependencies between input channels or spatial positions with minimal computational cost. Triplet Attention consists of three branches, each responsible for capturing the interaction features between the spatial dimensions H or W and the channel dimension C. By applying permutation transformations to the input tensors in each branch, followed by Z-pooling and a convolutional layer of size $k \times k$, attention weights are generated. These weights are then generated through a sigmoid activation layer and applied to the permuted input tensors, which are transformed back to their original input shape. Triplet Attention innovatively captures the interactions between the channel, height, and width dimensions by rotating the input tensors and applying residual transformations, thereby establishing dependencies among different dimensions.

The specific structure of the Triplet Attention mechanism is shown in Figure 5.

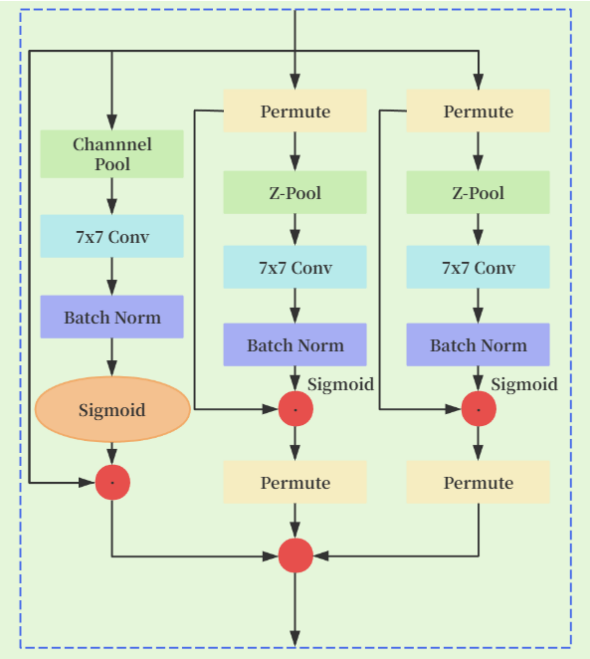

Figure 5. Structure of Triplet Attention

From Figure 5. , it can be observed that the structure is divided into three branches, each performing different operations: a 7×7 convolution after channel pooling, Z-pooling, followed by another 7×7 convolution, batch normalization, and a Sigmoid function. Each branch includes a Permute operation to adjust the dimensions. Finally, the results from the three branches are aggregated through average pooling to generate the final attention weights.

Each module is designed to process feature maps $(C \times H \times W)$, where C is the number of channels, H is the height, and W is the width. These modules compute attention weights in different ways, enhancing the network's focus on important parts of the features, thereby improving performance in various visual tasks.

We integrated the Triplet Attention mechanism into the C2PSA module of YOLOv11, proposing the C2PSA-TriAtt module, which achieves a dual improvement in computational efficiency and accuracy. The specific structure of the C2PSA-TriAtt module is shown in Figure 6.

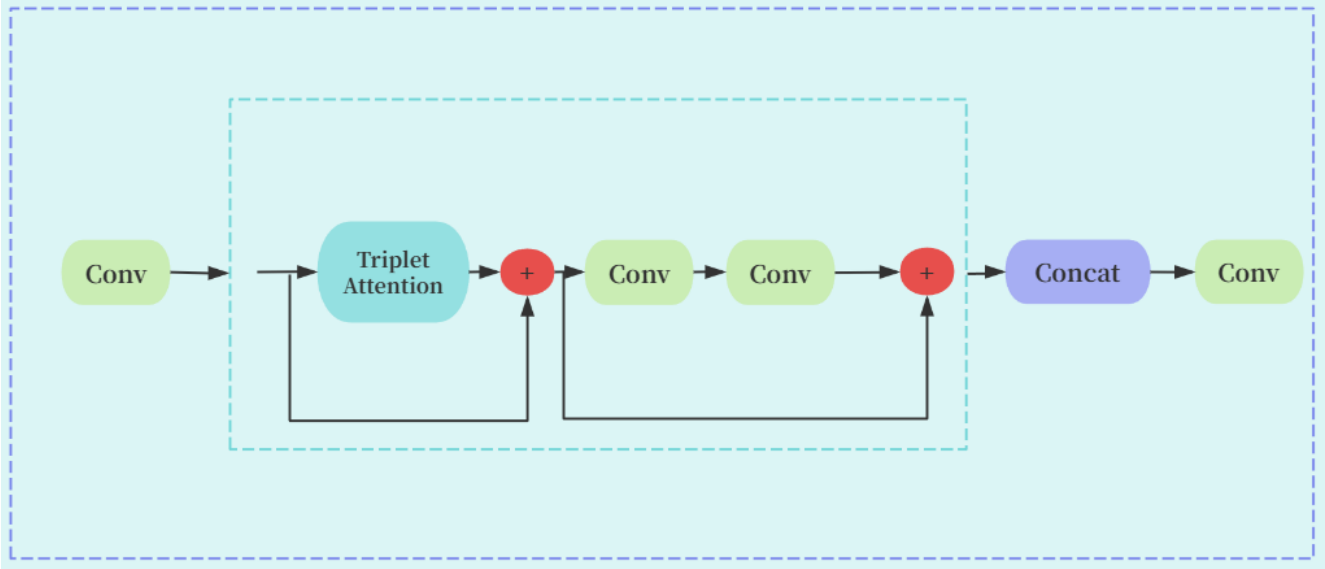

Figure 6. Structure of the C2PSA-TriAtt Module

2.5. ADown

To overcome the information bottleneck issue, a network structure named Programmable Gradient Information (PGI) was proposed in the lightweight down sampling operation ADown [28]. PGI primarily consists of three components: the main branch for inference, the auxiliary reversible branch for generating reliable gradients to supply the main branch for backpropagation, and the multi-level auxiliary information for controlling the main branch to learn multi-level semantic information. The goal of PGI is to address the information bottleneck problem through the auxiliary reversible branch, thereby providing more reliable gradients to deep networks without increasing the inference cost. With this design, even lightweight and shallow neural networks can achieve effective information retention and accurate gradient updates. As shown in the dark boxes in the figure, the main branch can obtain more effective task-relevant features by utilizing the reliable gradient information provided by the auxiliary reversible branch, without losing important information due to the information bottleneck.The specific network structure of PGI is shown in Figure 7.

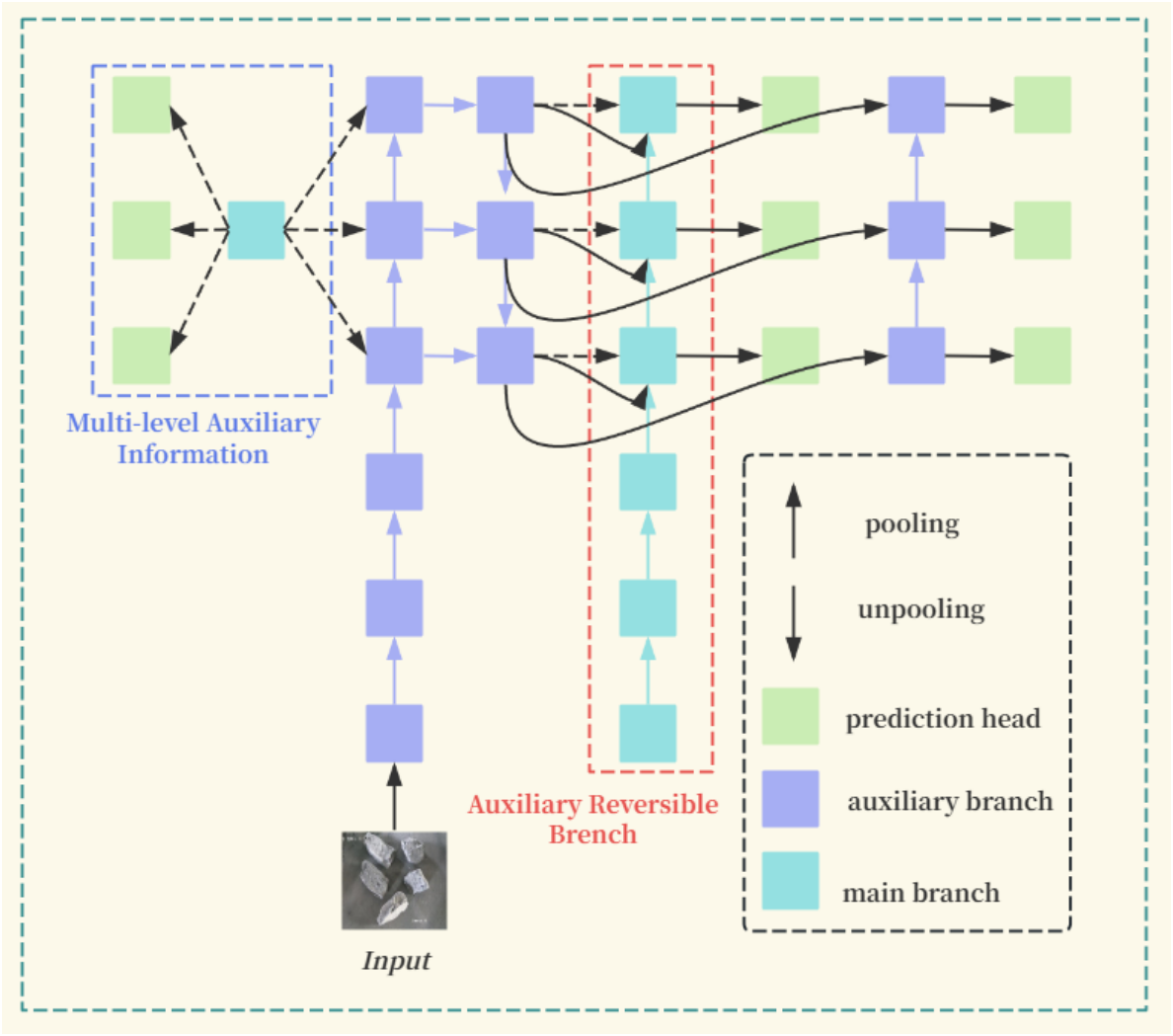

Figure 7. Reversible Programming Information (PGI) network structure

The expression for information loss due to the information bottleneck is given by Eq. 2.

$$I(X,X) \geq I(X,f_\theta(X)) \geq I(X,g_\emptyset(f_\theta(X))) \quad (2)$$

PGI mainly consists of three parts: the main branch, the auxiliary reversible branch, and the multi-level auxiliary information. From Figure 7. , we can see that the inference process of PGI only uses the main branch, thus incurring no additional inference cost. The other two parts are used to address or mitigate several important issues in deep learning methods.

Auxiliary Reversible Branch: This part aims to handle problems caused by deepening the neural network. Deepening the network leads to an information bottleneck, which makes it difficult for the loss function to generate reliable gradients.

Multi-Level Auxiliary Information: This part aims to address the error accumulation problem caused by deep supervision, especially for architectures with multiple prediction branches and lightweight models. To solve the issue of reversible architecture performing poorly in shallow networks compared to deeper networks when complex tasks require deeper transformations, PGI does not force the main branch to retain complete original information. Instead, it generates useful gradients through auxiliary supervision mechanisms to update the main branch. The advantage of this design is that the proposed method can also be applied to shallower networks. Finally, since the auxiliary reversible branch can be removed during the inference stage, the original network's inference capability is preserved. Additionally, any reversible architecture can be chosen to serve as the auxiliary reversible branch in PGI.

Within PGI, u and r represent the reversible functions, while φ and δ represent the parameters of these reversible functions. The expression that ensures the data X does not lose information through reversible function transformations is giv

en by Eq. 3.

$$I(X,X) = I\left(X, r_\varphi(X)\right) = I\left(X, u_\delta\left(r_\varphi(X)\right)\right) \quad (3)$$

The concept of multi-level auxiliary information involves inserting an integration network between the feature pyrami d layers of auxiliary supervision and the main branch. This i ntegration network is then used to combine the gradients ret urned from different prediction heads, as shown in Figure 7. Subsequently, the multi-level auxiliary information aggregat es the gradient information containing all target objects and passes it to the main branch to update the parameters. At this point, the characteristics of the feature pyramid levels in the main branch are not dominated by information from specific objects. Therefore, PGI can alleviate the broken information problem in deep supervision. Additionally, any integration n etwork can be used in the multi-level auxiliary information. Through this design, higher accuracy detection can be achie ved at a lower computational cost.

2.6. Inner-FocalerIoU

To improve the accuracy of bounding box regression (BB R) in object detection, especially when dealing with highly overlapping targets, Zhang et al. [29] proposed InnerIoU. Th is method calculates the loss function by introducing auxilia ry bounding boxes, which are reduced versions of the origin al bounding boxes. The advantages of these methods include the following four points:

1. Targeted Optimization: Inner-IoU provides a more preci se assessment of overlapping areas by focusing on the c ore part of the bounding box rather than the entire box.
2. Scale Adjustment: By controlling the size of the auxiliar y bounding boxes, Inner-IoU allows for fine-tuning for different datasets and detection tasks.
3. Improved Generalization: Experiments have shown that InnerIoU exhibits better generalization performance on different datasets compared to traditional IoU.
4. Handling High and Low IoU Samples: For high IoUsam ples, using smaller auxiliary boxes can accelerate mode l learning, while for low IoU samples, using larger auxil iary boxes can improve regression performance.

Inner-IoU is a more refined and center-focused performan ce evaluation metric that enhances the precision and efficien cy of object detection tasks through scale adjustment of auxi liary boxes.

The specific description of Inner-IoU is illustrated in Figu re 8.

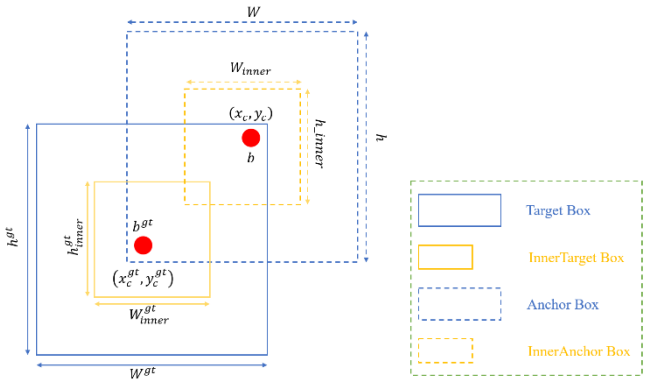

Figure 8. Description of Inner-IoU

As shown in Figure 8. , the ground truth box and the anch or box are denoted as b^{gt} and b, respectively. The centers of the GT box and the inner GT box are represented by the poi nt (x_c^{gt}, y_c^{gt}), while the centers of the anchor box and the in ner anchor box are denoted by (x_c, y_c). The width and heigh t of the GT box are denoted as w^{gt} and h^{gt}, respectively, an d the width and height of the anchor box are denoted as w a nd h. The variable "$ratio$" corresponds to the scaling factor, t ypically within the range [0.5, 1.5].

Inner-IoU is calculated from both the intersection (inter) a nd the union. The formula for calculating the $inter$ is given by Eq. 4.

$$inter = \left(\min\left(b_r^{gt}, b_r\right) - \max\left(b_l^{gt}, b_l\right)\right) * \left(\min\left(b_b^{gt}, b_b\right) - \max\left(b_t^{gt}, bt\right)\right) \quad (4)$$

The calculation formulas for other parameters included in Eq. 4 are shown below.

$$b_l = x_c - \frac{w * ratio}{2}, \qquad b_r = x_c + \frac{w * ratio}{2} \quad (5)$$

$$b_t = y_c - \frac{h * ratio}{2}, \qquad b_b = y_c + \frac{h * ratio}{2} \quad (6)$$

$$b_l^{gt} = x_c^{gt} - \frac{w^{gt} * ratio}{2}, \qquad b_r^{gt} = x_c^{gt} + \frac{w^{gt} * ratio}{2} \quad (7)$$

$$b_t^{gt} = y_c^{gt} - \frac{h^{gt} * ratio}{2}, \qquad b_b^{gt} = y_c + \frac{h * ratio}{2} \quad (8)$$

The calculation formula for $union$ is shown in Eq. 9.

$$union = (s^{gt} * h^{gt}) * (ratio)^2 + (w * h) * (ratio)^2 - inter \quad (9)$$

Combining the above formulas, the expression for IoU^{inner} can be derived, as shown in Eq. 10.

$$IoU^{inner} = \frac{inter}{union} \quad (10)$$

To focus on different regression samples and address the issue of the distribution of difficult and easy samples, Zhang et al. [30] proposed Focaler-IoU. Focaler-IoU enhances detector performance across various detection tasks by focusing on different regression samples. This is achieved through a linear interval mapping that reconstructs the IoU loss to focus on different samples. It analyzes and considers the distribution of difficult and easy samples in bounding box regression, which is an aspect often overlooked in traditional IoU loss functions. Focaler-IoU compensates for the shortcomings of existing bounding box regression methods through its unique approach, further improving detection performance across different tasks. The specific expression of $IoU^{focaler}$ is given in Eq. 11.

$$IoU^{focaler} = \begin{cases} 0, & IoU < d \\ \dfrac{IoU - d}{u - d}, & d \ll IoU \ll u \\ 1, & IoU > u \end{cases} \quad (11)$$

As shown in Eq. 11, the loss function adjusts based on the Intersection over IoU value. Specifically, if the IoU is less than a lower threshold *d*, the loss is set to 0. When the IoU exceeds an upper threshold *u*, the loss is set to 1. For IoU values between *d* and *u*, the loss increases linearly with the IoU value. This design allows the loss function to be sensitive to IoU values within a specific range, enabling it to focus more on samples with moderate overlap between the predicted and ground truth bounding boxes—samples that areneither too difficult nor too easy. This helps the model betterlearn to extract features from moderately difficult samples rather than focusing solely on the easiest or hardest samples.

Building on the findings of the aforementioned studies, we combined Inner-IoU with Focaler-IoU to propose Inner-FocalerIoU. The expression for $IoU_{inner}^{focaler}$ is shown in Eq. 12.

$$IoU_{inner}^{focaler} = \begin{cases} 0, & IoU < d \\ \dfrac{IoU_{inner} - d}{u - d}, & d \ll IoU \ll u \\ 1, & IoU > u \end{cases} \quad (12)$$

3. Experiments and Data Analysis

3.1. Data Collection and Preprocessing

The experiments rely on an independently collected dataset of coal and gangue images for training. Specifically, to gather the image data of coal and gangue, videos of coal and gangue were recorded under different lighting conditions using a dark background. Frames were then extracted from these videos, and each frame was carefully annotated. In total, 3091 images were collected, and these images were divided into a training set, a test set, and a validation set according to a *0.7:0.15:0.15* strategy. This means that 2164 images were used for training, 463 images for testing, and 464 images for validation.

3.2. Experimental Setup

The experiments were conducted using the Pytorch 2.2.0 framework on a Windows operating system. The hardware configuration includes an AMD Ryzen 7 4800H with Radeon Graphics CPU with a frequency of 2.90 GHz, an NVIDIA GTX1650Ti GPU, and 16 GB of RAM. The input image size was set to *640×640*, and image input used 2 threads. The batch size was 8, and the weight decay parameter was set to 0.0005. The training was performed for 200 epochs with a learning rate of 0.01. The evolution hyperparameter catch was set to false, and no pre-trained model was used. Data augmentation was performed using the default mosaic augmentation strategy.

The specific training process of the model is illustrated in Figure 9.

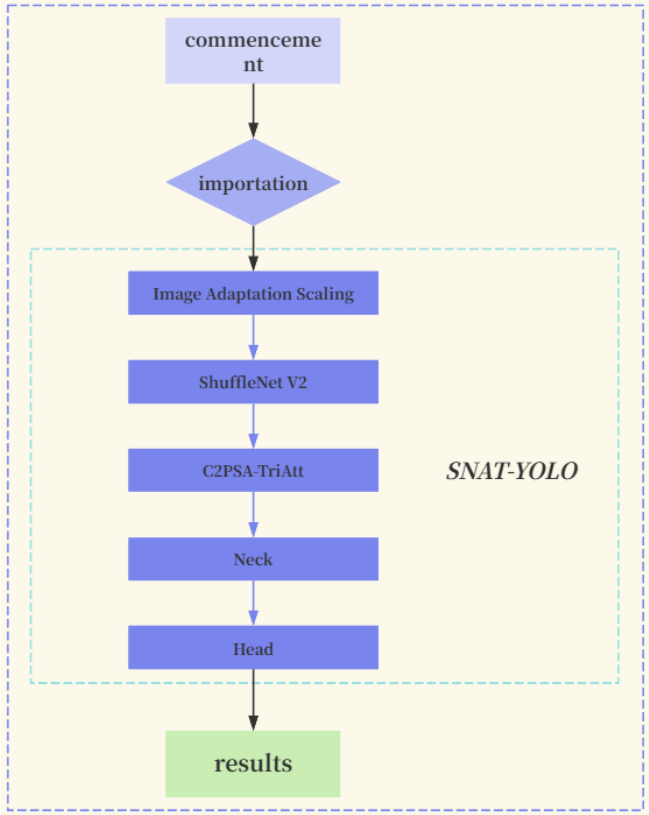

Figure 9. Model Training Process

To evaluate the performance of the gangue detection algorithm, we used several metrics including model size (Size),

number of parameters (Params), floating-point operations (GFLOPs), mean detection time (MDT), mean Average Precision (mAP), and mAP50-95 (model average precision at confidence thresholds from 0.50 to 0.95). Unlike mAP50, mAP50-95 considers a broader range of IoU, allowing for the assessment of the model's performance across different overlap thresholds. The GFLOPs metric represents the model's computational complexity, with a higher GFLOPs indicating greater computational resource requirements.

The MDT is derived from the frames per second (FPS). The formula for calculating FPS is shown in Eq. 13.

$$FPS = \frac{1 \times 10^3}{preprocess + inference + postprocess} \quad (13)$$

As a performance metric, MDT (Mean Detection Time) represents the average detection time per image when the model performs the detection task. The formula for calculating MDT is shown in Eq. 14.

$$MDT = \frac{1}{FPS} \quad (14)$$

As a performance metric, mAP50 (mean Average Precision at an Intersection over IoU threshold of 50%) represents the average precision of the model when the IoU is set to 50. The formula for calculating mAP is shown in Eq. 15.

$$mAP = \frac{1}{n}\sum_{k=1}^{k=n} AP_k \quad (15)$$

3.3. Comparative Experiments

To validate the performance improvements of the proposed algorithm, we conducted a comparison between the improved algorithm and several state-of-the-art models, including YOLOv5, YOLOv8, YOLOv9, YOLOv10, YOLOv11, the Yolov8n-FEL proposed by Yan et al. [33], and the Our-Yolo algorithm proposed by Zeng et al. [23]. The hyperparameters and training parameters for all models were set to their default values. The detailed comparison results are shown in Table 1.

Table 1. Performance Comparison of Different Algorithm Models

model	Parameters(M)	MDT(ms)	GFLOPs	mAP50(%)	Size(MB)
YOLOv5	2.50	6.2	7.1	98.10	5.03
YOLOv8n	3.01	7.8	8.1	98.50	6.31
YOLOv9t	1.97	10.0	7.6	97.90	4.43
YOLOv10n	2.69	7.5	8.2	97.40	5.49
YOLOv11	2.59	8.4	6.3	98.10	5.22
Our-v8[23]	12.8	8.0	29.7	**99.50**	22.10
Yolov8n-FEL[32]	2.55	**4.4**	6.8	98.90	5.07
SNAT-YOLO(Ours)	**1.52**	7.4	**3.8**	99.10	**3.25**

From Table 1. , it is evident that our proposed algorithm achieves the best performance in terms of the number of parameters, GFLOPs, and model size. Compared to YOLOv5, YOLOv8n, YOLOv9t, YOLOv10n, and YOLOv11, our proposed algorithm consistently outperforms these models across all metrics.When compared to Our-v8, although it outperforms our model in the mAP50 metric, our model significantly reduces the number of parameters by 88%, the GFLOPs by 87%, and the model size by 85%, while only experiencing a 0.4% decrease in detection accuracy.In comparison with another lightweight model, Yolov8n-FEL, our model maintains a similar detection accuracy while reducing the number of parameters by 40%, the GFLOPs by 44%, and the model size by 36%.

Therefore, our model not only maintains high detection accuracy but also significantly reduces the dependence on computational resources.

3.4 Ablation Experiments

To validate the effectiveness of each individual enhancement in our improved algorithm, we conducted ablation experiments to visually demonstrate the efficiency improvements brought about by each module. The detailed ablation experiment results are shown in Table 2. YOLOv11 represents the baseline version without any modifications; S-YOLO represents the version where the backbone of YOLOv11 is replaced with the ShuffleNetV2 network; ST-YOLO represents the version where the original C2PSA module in S-YOLO is replaced with our proposed C2PSA-TriAtt module; STA-YOLO represents the version where the ADown down sampling operation is incorporated into ST-YOLO; STAIF-YOLO represents the version where the original CIoU loss function in

STA-YOLO is replaced with our proposed Inner-FocalerIoU loss function.

Table 2. Ablation Experiment Results

Model	GFLOPs	Parameters(M)	MDT(ms)	Size(MB)	mAP50(%)	mAP50-95(%)
YOLOv11	6.3	2.59	8.4	5.22	0.981	0.832
S-YOLO	4.1	1.70	7.6	3.60	0.978	0.829
ST-YOLO	4.0	1.65	7.7	3.50	0.983	0.833
STA-YOLO	3.8	1.52	7.9	3.25	0.988	0.837
STAIF-YOLO	3.8	1.52	7.4	3.25	0.991	0.839

From Table 2. , it is evident that the detection accuracy of the unmodified YOLOv11 network is 98.1%, with 2.59M parameters, 119 FPS (resulting in an average detection time of 8.4ms per image), and 6.3 GFLOPs. After replacing the backbone of YOLOv11 with the ShuffleNetV2 network, the number of parameters was reduced by 34%, the model size by 31%, and the GFLOPs by 34%. This reduction is attributable to ShuffleNetV2's emphasis on not only accuracy but also speed, memory access cost, and platform characteristics. ShuffleNetV2 employs pointwise group convolution and channel shuffle operations to maintain network accuracy while significantly reducing computational costs. To adapt to mobile deployment, ShuffleNetV2 reduces model fragmentation and minimizes element-wise operations, contributing to model lightweighting. Although the model's accuracy slightly decreased after integrating ShuffleNetV2, the improvements in speed and efficiency outweigh this drawback. After incorporating the C2PSA-TriAtt module, the model's accuracy improved to 98.6%, and compared to S-YOLO, the number of parameters decreased by 7%, the model size by 2%, and GFLOPs further reduced to 4.0. This improvement is due to Triple Attention, which captures cross-dimensional interactions in the input data using three branches. Each branch calculates attention weights across dimensions, constructing dependencies between channels and spatial positions at a minimal computational cost. This design enables the model to better capture interactions between spatial and channel dimensions, enhancing feature comprehension. Specifically, the mAP50 and mAP50-95 metrics increased to 98.3% and 83.3%, respectively, surpassing the unmodified YOLOv11, thanks to Triple Attention's ability to focus on spatial dimensions. The integration of ADown, a novel lightweight down sampling operation, further enhanced the network's Neck module. ADown introduces gradient programming information (PGI) to address information bottlenecks effectively, ensuring reliable gradient updates without increasing inference costs. Lightweighting is achieved through the GELAN architecture, offering a more general and efficient network for tasks ranging from lightweight to complex, while maintaining or enhancing computational efficiency and performance. After incorporating ADown, the model's detection accuracy increased to 98.8%, GFLOPs decreased to 3.8, and compared to ST-YOLO, the number of parameters decreased by 7.8%, and the model size by 7.1%. Finally, replacing the original CIoU with Inner-FocalerIoU resulted in a slight improvement in mAP50 (99.1%) and mAP50-95 (83.9%) compared to STA-YOLO, thanks to Inner-FocalerIoU's ability to address sample imbalance and accuracy degradation issues during high object overlap. Overall, our proposed SNAT-YOLO model achieves a 40% reduction in GFLOPs, a 41% reduction in parameters, and a 38% reduction in model size compared to the unmodified YOLOv11, while increasing mAP50 by 1% and mAP50-95 by 0.7%. This demonstrates that our model maintains high detection accuracy while significantly improving lightweighting, making it more suitable for deployment on industrial edge devices.

3.5. Results Presentation

The experimental results demonstrate that SNAT-YOLO exhibits high detection accuracy and short detection time. The following figure displays the detection results of SNAT-YOLO on the test dataset. It can be observed that SNAT-YOLO can accurately identify and locate targets even in coal and rock images that are difficult for humans to quickly and accurately assess. Moreover, SNAT-YOLO demonstrates favorable recognition performance across different volumes of coal and rock, thus playing a significant role in coal and rock separation.

As shown in Figure 10. , the bounding boxes depict the coal and rock identified by SNAT-YOLO, with the specific target types displayed at the top left corner of each bounding box. By utilizing the two coordinates of the identification boxes, the relative position of the entire target with respect to the image can be obtained, which is beneficial for the subsequ

ent separation of coal and rock.

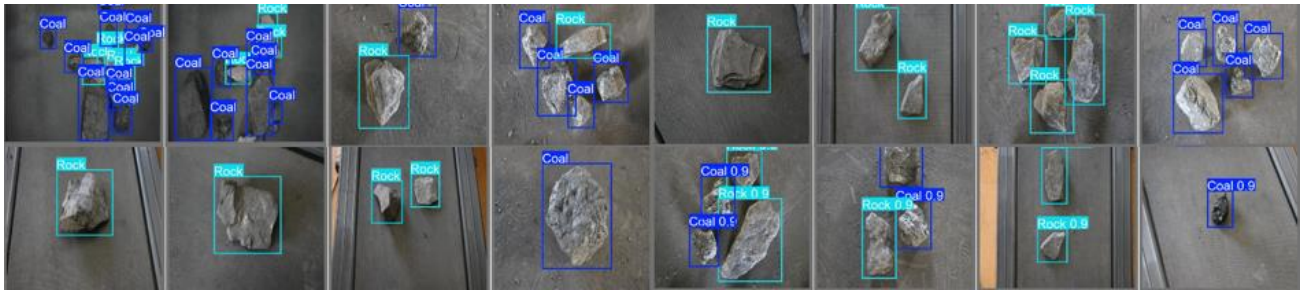

Figure 10. Coal and Gangue Detection Results

4. Conclusion

In this paper, we propose a coal and rock recognition method based on an improved YOLOv11 network structure. This method not only ensures high detection accuracy but also significantly improves detection efficiency, enabling real-time detection of coal and rock in complex underground environments. By saving a substantial amount of human and material resources, this method promotes the efficient utilization of coal resources and holds significant importance for the future intelligent mining of coal.

To enhance the quality of the dataset, we meticulously annotated 3,091 coal and rock images and further optimized the data using data augmentation techniques. To reduce the computational load of the model, we replaced the backbone network of YOLOv11 with ShuffleNetV2 and introduced the Triplet Attention self-attention mechanism into the C2PSA module, resulting in the proposed C2PSA-TriAtt module. Additionally, we integrated the lightweight down sampling operation ADown into the neck structure of YOLOv11, which not only improved the computational efficiency of the model but also significantly enhanced detection accuracy. Furthermore, we introduced the Inner-FocalerIoU loss function to replace the original CIoU loss function, significantly improving the accuracy of bounding box regression (BBR) and effectively addressing the issue of imbalanced sample distribution.

The results show that, compared to current mainstream object detection algorithms, our improved YOLOv11 model achieves higher detection accuracy and faster detection speed. This model can be deployed on industrial edge devices in complex environments, contributing to the advancement of coal mining and the utilization of coal resources.

In future research, considering the diverse conditions in actual production environments, we plan to collect coal and rock datasets from different production scenarios, including but not limited to dusty environments and low-light conditions, to enhance the generalization performance of the model. We will also design specific network structures for different production scenarios to ensure the efficient application of the model in actual production. Furthermore, we plan to integrate our algorithmic model with mechanical sorting devices to further facilitate the practical application of our research findings in production.

Data availability

The datasets generated during and/or analysed during the current study are available from the corresponding author on reasonable request.

References

[1]. Yuan L, Wang E, Ma Y, et al. Research progress of coal and rock dynamic disasters and scientific and technological problems in China[J]. Journal of China Coal Society, 2023, 48(5): 1825-1845.

[2]. Shi L, Peng J, Xu D, et al. Leaching characteristics and pollution risk assessment of potentially harmful elements from coal gangue exposed to weathering for different periods of time [J]. Environmental Science and Pollution Research, 2023, 30 (22): 63200-63214.

[3]. Tang T , Wang Z , Chen L ,et al.Opportunities, challenges and modification methods of coal gangue as a sustainable soil conditioner—a review[J].Environmental Science & Pollution Research, 2024, 31(48).DOI:10.1007/s11356-024-34895-2.

[4]. Ruxin G , Yabo D , Tengfei W .Research on coal gangue classification recognition method based on the combination of CNN and SVM[J].Journal of Real-Time Image Processing, 2023(6):20.

[5]. Sui Y. Study on Ecological Environment Compensation Based on the Analysis of Ecological Footprint in Coal Mine[J]. CHINA UNIVERSITY OF MINING AND TECHNOLOGY, 2015.

[6]. Gao L, Liu Y, Xu K, et al. A short review of the sustainable utilization of coal gangue in environmental applications[J]. RSC advances, 2024, 14(53): 39285-39296.

[7]. Zheng Q, Zhou Y, Liu X, et al. Environmental hazards and comprehensive utilization of solid waste coal gangue[J]. Progress in Natural Science: Materials International, 2024.

[8]. Pan W, Guo J. Technical transformation plan and economic analysis of manual selection workshop in coal preparation plant[J]. China Energy Environ Protect, 2018, 40: 154-158.

[9]. Zhang Y, Zhu H, Zhu J, et al. Experimental study on separation of lumpish coal and gangue using X-ray[J]. Energy Sources, Part A: Recovery, Utilization, and Environmental Effects, 2021: 1-13.

[10]. Kehong Z , Changlong D , Jianping L ,et al.Coal and Gangue Underground Pneumatic Separation Effect Evaluation Influenced by Different Airflow Directions[J].Advances in Materials Science and Engineering,2016,(2016-3-17), 2016, 2016:1-13.DOI:10.1155/2016/6465983.

[11]. Yin J , Zhu J , Zhu H ,et al.Intelligent photoelectric identification of coal and gangue A review[J].Measurement, 2024, 233. DOI:10.1016/j.measurement.2024.114723.

[12]. Xu J , Wang F .Study of Automatic Separation System of Coal and Gangue by IR Image Recognition Technology[C]//International Conference on Automation and Robotics.2011.

[13]. Dwari R K, Rao K H. Dry beneficiation of coal—a review[J]. Mineral Processing and Extractive Metallurgy Review, 2007, 28(3): 177-234.

[14]. WANG Y, GUO D, ZHANG H, et al. Spatial distribution and applications of coal resource potential in China[J]. Journal of natural resources, 2006, 21(2): 226-230.

[15]. Gui X, Liu J, Cao Y, et al. Coal preparation technology: Status and development in China[J]. Energy & Environment, 2015, 26(6-7): 997-1013.

[16]. Brodtkorb A R, Hagen T R, Sætra M L. Graphics processing unit (GPU) programming strategies and trends in GPU computing[J]. Journal of Parallel and Distributed Computing, 2013, 73(1): 4-13.

[17]. Xin F, Jia Q, Yang Y, et al. A high accuracy detection method for coal and gangue with S3DD-YOLOv8[J]. International Journal of Coal Preparation and Utilization, 2024: 1-19.

[18]. Lei S, Xiao X, Zhang M. Research on coal gangue identification method based on improved yolov3[J]. Mining Safety & Environmental Protection, 2021, 48(03): 50-55.

[19]. Sui Y , Zhang L , Sun Z ,et al.Research on Coal and Gangue Recognition Based on the Improved YOLOv7-Tiny Target Detection Algorithm[J].Sensors (14248220), 2024, 24(2).DOI: 10.3390/s24020456.

[20]. Zhang, S. et al. Research on coal gangue recognition based on improved YOLOv5. Ind. Min. Autom. 48(11), 39–44.

[21]. Chang, F. Y. & Zhao, G. Coal gangue identification method based on YOLOv5m improved model. Coal Technol. 42(07), 10–14.

[22]. Shen, K. et al. Coal gangue target detection based on improved Yolov5s model. Ind. Min. Autom. 47(11), 107–111+118.

[23]. Zeng Q , Zhou G , Wan L ,et al.Detection of Coal and Gangue Based on Improved YOLOv8[J].Sensors (14248220), 2024, 24(4).DOI:10.3390/s24041246.

[24]. Jegham N, Koh C Y, Abdelatti M, et al. Evaluating the evolution of yolo (you only look once) models: A comprehensive benchmark study of yolo11 and its predecessors[J]. arXiv preprint arXiv:2411.00201, 2024.

[25]. Hidayatullah P, Syakrani N, Sholahuddin M R, et al. YOLOv8 to YOLO11: A Comprehensive Architecture In-depth Comparative Review[J]. arXiv preprint arXiv:2501.13400, 2025.

[26]. Du S, Zhang B, Zhang P, et al. An improved bounding box regression loss function based on CIOU loss for multi-scale ob

ject detection[C]//2021 IEEE 2nd International Conference o n Pattern Recognition and Machine Learning (PRML). IEEE, 2021: 92-98.

[27]. Ma N , Zhang X , Zheng H T ,et al.ShuffleNet V2: Practical Guidelines for Efficient CNN Architecture Design[J].Springe r, Cham, 2018.DOI:10.1007/978-3-030-01264-9_8.

[28]. Wang C Y , Yeh I H , Mark Liao H Y .YOLOv9: Learning W hat You Want toLearn Using Programmable Gradient Inform ation[C]//European Conference on Computer Vision.Springe r, Cham, 2025.DOI:10.1007/978-3-031-72751-1_1.

[29]. Zhang H , Xu C , Zhang S .Inner-IoU: More Effective Inters ection over Union Loss with Auxiliary Bounding Box[J]. 20 23.

[30]. Zhang, H., & Zhang, S. (2024). Focaler-IoU: More Focused Intersection over Union Loss. *ArXiv, abs/2401.10525*.

[31]. Misra D , Nalamada T , Arasanipalai A U ,et al.Rotate to Atte nd: Convolutional Triplet Attention Module[J]. 2020.DOI:10. 48550/arXiv.2010.03045.

[32]. Yan P, Wang W, Li G, et al. A lightweight coal gangue detect ion method based on multispectral imaging and enhanced Y OLOv8n[J]. Microchemical Journal, 2024, 199: 110142.

.